HYDROGEN, FUEL CELL & ENERGY STORAGE

Applying geothermal and solar energies for the thermodynamic estimation of the multigeneration system's performance in producing power, freshwater and hydrogen

Eman Shakir Hussein Hussein | Iraj Mirzaee* | Samrand Rash-Ahmadi | Morteza Khalilian

Mechanical Engineering Department, Engineering Faculty, Urmia University, Urmia, Iran
* Corresponding author, Email: i.mirzaee@urmia.ac.ir

Article Information

Article Type
Research Article

Article History
Received: *25 Jun 2024*
Revised: *23 Aug 2024*
Accepted: *01 Sep 2024*
Published Online: *01 Sep 2024*

Keywords
Solar and geothermal energy
Hydrogen
Thermodynamic analysis
Freshwater
Power

Abstract

The evaluation in the study includes assessing the energy and exergy of a novel system capable of producing cooling, heat, electricity, hot water, hydrogen, and desalinated water simultaneously. This groundbreaking system utilizes solar and geothermal energy and consists of a proton exchange membrane (PEM) electrolyzer, reverse osmosis (RO) desalination unit, an organic Rankine cycle (ORC), an absorption refrigeration cycle, and a domestic water heater. The EES software was used to perform all the analyses. An examination of the proposed system was carried out, considering both energy and exergy aspects. The results indicate that the solar collector undergoes the most exergy destruction when examined. As the volume concentration of nanoparticles increases, the turbine's power production increases, while the thermoelectric generator's (TEG) power generation decreases. The solar collector's useful energy increases with higher solar irradiation but decreases as the nanoparticle percentage rises. The turbine and TEG unit produce more power when exposed to greater solar irradiation, resulting in higher rates of freshwater and hydrogen production.

Cite this article: Hussein, E. S. H., Mirzaee, I., Rash-Ahmadi, S., Khalilian, M. (2024). Applying geothermal and solar energies for the thermodynamic estimation of the multigeneration system's performance in producing power, freshwater and hydrogen. DOI: 10.22104/HFE.2024.6948.1302

 Publisher: Iranian Research Organization for Science and Technology (IROST)
DOI: 10.22104/HFE.2024.6948.1302

1 Introduction

The global energy reserves are projected to diminish by 60% by 2030, according to the International Energy Agency, while energy demand is expected to increase [1]. As a result, there is a growing emphasis on renewable energy, driven by escalating oil and gas prices, constraints on resources, environmental worries, and climate change. Renewable energy sources, like sunlight, wind, rain, tides, and geothermal heat, are naturally replenished over time. Unlike finite fossil fuels, renewable energy sources can be continually and sustainably utilized. They offer several advantages over traditional fuels, including reduced carbon emissions, improved air and water quality, and increased energy independence.

Renewable resources have the benefit of being widely available across different regions, which means that they can provide electricity for developing areas at a stable and long-lasting cost. These resources include solar, wind, and hydroelectric power. Solar power harnesses the heat of the sun, which also creates the winds that can be captured by wind turbines. Additionally, the sun's heat and the winds contribute to water evaporation and precipitation formation. This precipitation can flow down rivers or streams, providing the basis for generating hydroelectric power [2].

Renewable energy has numerous advantages, including its sustainability, widespread availability (unlike fossil fuels and minerals), and minimal pollution. The generation of electricity from renewable sources like wind turbines and photovoltaic panels does not depend on water, unlike steam plants powered by fossil fuels and nuclear energy [3]. Solar energy is widely recognized as a crucial renewable source due to its cleanliness and abundance [4]. Among renewable energy sources, solar power ranks highly in its capacity to generate electricity. Solar collectors are critical components in harnessing solar energy directly by capturing solar radiation and converting it into heat for various applications, including generating electricity. [5]. Solar collectors are the most crucial component in any solar thermal system. Geothermal energy, generated from the natural heat of the Earth's core, is another type of renewable energy. It is naturally created and stored within the Earth. Geothermal energy is known for its lower costs, widespread availability, and clean characteristics [6].

Multigeneration systems are the systems that can produce more than three products by using one or more energy systems. Because of their excellent performances, they have garnered significant attention from researchers.

Sezer and colleagues [7] developed a new renewable energy-based 'multi-generation' system that can generate hydrogen, oxygen, desalinated water, and cooling in addition to electricity. The study revealed that the overall power and energy efficiencies were 73.3% and 30.6%, respectively. The researchers also calculated the exergy destruction rates of the system's components. In conclusion, combining multiple sustainable energy sources in a single system guarantees the production of various resources through an eco-friendly process.

Bicer and Dincer [8] put forward and examined an integrated system capable of generating power, providing cooling, heating, and producing hydrogen in their research. The system incorporated parabolic trough collectors (PTC) for generating electricity and meeting various requirements in a multi-generation setup. By utilizing geothermal water at a temperature of 210 ℃, the system can attain overall energy and exergy efficiencies reaching up to 10.8% and 46.3%, respectively.

Alirahmi and colleagues [9] designed a system with the ability to produce hydrogen, fresh water, electricity, cooling capacity, and hot water. Through experimentation with different fluids, it was observed that syltherm800 demonstrated promising characteristics. A thorough parametric study was carried out by the researchers to analyze the influence of various factors on the system's overall efficiency. The increase in solar collector area from 5000 to 25,000 m^2 led to a rise in power output from 702 kW to 3512 kW, accompanied by an increase in cost from 34.72 to 151.5$/h. The research findings indicated that with an increase in solar radiation intensity from 300 W/m^2 to 900 W/m^2 for geothermal fluid at 110 °C, the production of hydrogen rose from 0.638 kg/h to 1.958 kg/h, and the output of freshwater escalated from 8.61 m^3/h to 27.46 m^3/h. The results clearly showed that the primary source of exergy destruction was linked to PTCs and absorption chillers.

Yuksel and Ozturk [10] presented a novel multigeneration system capable of producing hydrogen, electricity, cooling, heating, and domestic hot water in their research. They proceeded to analyze the system from the perspectives of energy, exergy, and thermoeconomics, uncovering that the system achieved an overall energy efficiency of 47.04% and an exergy efficiency of 32.15%.

Wan et al. [11] designed a new hybrid geothermal-solar flash-binary system. The system comprises a solar preheat subsystem, a flash-binary subsystem, and a binary subsystem. The research indicates that as the flash pressure increased, the thermodynamic performance of the system improved. Furthermore, the net power output and energy efficiency both peaked at an evaporation pressure of 1.5 MPa.

Ayub et al. [12] developed a comprehensive model for a hybrid solar-binary geothermal system that utilizes solar-through technology. They utilized the EES (Engineering Equation Solver) to implement the models. The primary emphasis of the optimization was on maximizing the total work output (W_{net}) of the hybrid system. To assess the economic performance of the hybrid system, they utilized the levelized electricity cost (LEC) as a measure. The results revealed a 2% reduction in LEC for the hybrid system compared to a standalone geothermal system. The technical and economic assessment of the hybrid system indicates its superiority over the individual combined systems.

A comparative study conducted by Assareh et al. [13] analyzed multi-generation systems that used geothermal and solar energy for producing electricity and hydrogen cleanly, with assessments of energy and exergy. The study, which focused on the ambient temperature of Bandar Abbas city, found that the geothermal system outperformed the solar system. In particular, it led to 11.21% higher hydrogen production and 0.17% higher exergy efficiency.

2 System description

Figure 1 illustrates the schematic of the system under study, which incorporates geothermal energy and solar energy as the main energy sources. This system also includes an ORC cycle, double-effect absorption refrigeration chiller, reverse osmosis system, and proton exchange membrane electrolyzer. Power generation in this system is carried out by the ORC cycle turbine and the TEG unit. Additionally, the double-effect absorption refrigeration chiller provides the necessary cooling, while the reverse osmosis (RO) unit and proton exchange membrane (PEM) electrolyzer are responsible for producing fresh water and hydrogen, respectively. The geothermal fluid is directed from the production well to the parabolic trough collector (PTC) solar collector for further energy utilization.

The ORC evaporator receives the hot geothermal fluid initially. In the steam cycle, a turbine is powered by the working fluid, which absorbs heat from the hot steam flow, with a steam generator located at point 2. Then, the remaining thermal energy of the hot water exiting the steam generator at point 3 drives the generator of an absorption cooling system. Subsequently, the steam produced is utilized to preheat the feed water of a PEM electrolyzer at point 40 through a domestic water heater (DWH). The reinjection well receives the geothermal fluid in the end. At the same time, the electric energy from the ORC cycle and the TEG unit is used to operate a reverse osmosis desalination system and a PEM electrolyzer. Freshwater and hydrogen for different uses are produced by these systems.

There are several equations necessary to model the studied system, including mass balance, energy balance, and exergy equations.

$$\sum \dot{m}_{\text{out}} + \frac{dm_{cv}}{dt} = \dot{m}_{\text{in}}\,, \tag{1}$$

$$\dot{Q} - \dot{W} + \sum_{\text{in}}\sum_{\text{out}} \dot{m}_{\text{out}}\left(h_{\text{out}} + \frac{V_{\text{out}}^2}{2} + gZ_{\text{out}}\right)\frac{dE_{cv}}{dt} = \dot{m}\left(h_{\text{in}} + \frac{V_{\text{in}}^2}{2} + gZ_{\text{in}}\right), \tag{2}$$

$$\dot{\text{E}}\text{x}_Q + \sum_{\text{in}} \dot{m}_{\text{in}}\text{ex}_{\text{in}} = \sum_{\text{out}} \dot{m}_{\text{out}}\text{ex}_{\text{out}} + \dot{\text{E}}\text{x}_W + \dot{\text{E}}\text{x}_D\,, \tag{3}$$

$$\dot{\text{E}}\text{x}_{ph} = \sum \dot{m}_{\text{in}}\left[(h_{\text{in}} - h_{\text{out}}) - T_0(s_{\text{in}} - s_{\text{out}})\right]. \tag{4}$$

The PTC solar collector in this research uses a nanofluid composed of Therminol VP1 as the base fluid and Al_2O_3 nanoparticles. These nanoparticles were selected for their exceptional and varied physical characteristics, which surpass those of base fluids. The thermodynamic properties of these nanoparticles are provided in Table 1.

Table 1. Characteristics of nanoparticles under investigation [14].

Particle	ρ (kg/m^3)	k (W/m.K)	c_p (kJ/kg.K)
Al_2O_3	3970	40	0.765

The density, specific heat capacity, thermal conductivity and dynamic viscosity of nanofluids are presented as follows [15]:

$$\rho_{\text{nf}} = \varphi\rho_{\text{np}} + (1-\varphi)\rho_{\text{bf}}\,, \tag{5}$$

$$c_{p,\text{nf}} = \frac{\rho_{\text{np}}\varphi c_{p,\text{np}} + \rho_{\text{bf}}(1-\varphi)c_{p,\text{bf}}}{\rho_{\text{nf}}}\,, \tag{6}$$

$$k_{\text{nf}} = k_{\text{bf}}\frac{k_{\text{np}} + 2k_{\text{bf}} + 2(k_{\text{np}} - k_{\text{bf}})(1+\beta)^3\varphi}{k_{\text{np}} + 2k_{\text{bf}} - (k_{\text{np}} - k_{\text{bf}})(1+\beta)^3\varphi}\,, \tag{7}$$

$$\mu_{\text{nf}} = \mu_{\text{bf}}(1 + 2.5\,\varphi + 6.5\,\varphi^2)\,, \tag{8}$$

where φ is the nanoparticle volume concentration.

Parabolic trough collector The modeling of the solar system includes an energy and exergy analysis of the parabolic trough solar collector in this section [16]. The collector yields valuable power equivalent to:

$$Q_u = n_{\text{cp}}n_{\text{cs}}F_R A_{\text{ap}}\left[S - \frac{A_r}{A_{\text{ap}}}U_L(T_{r,i} - T_0)\right]. \tag{9}$$

In this equation, n_{cp} and n_{cs} represent the number of parallel and series collectors, respectively.

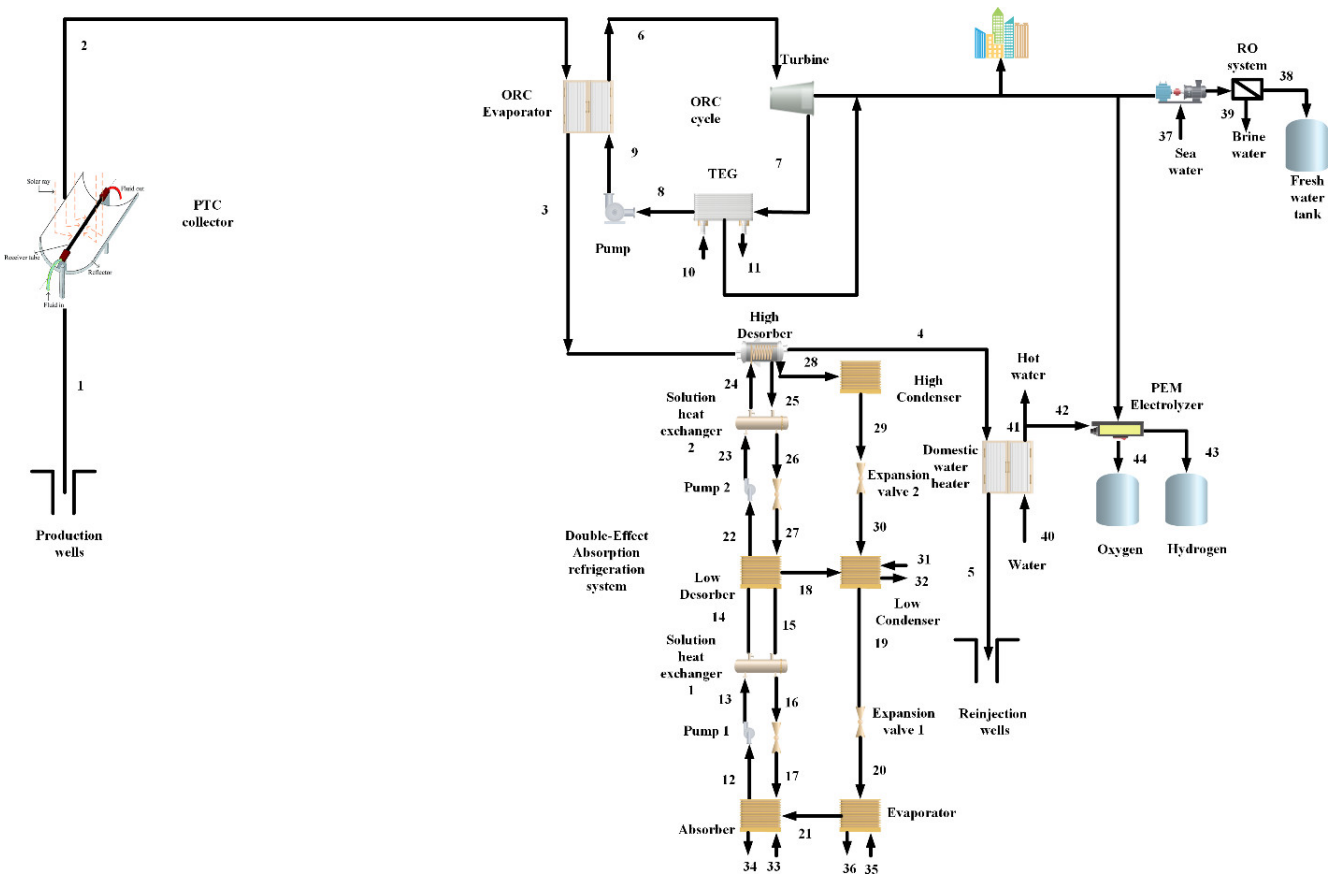

Fig. 1. Schematic displaying the proposed multigeneration system.

Also, A_{ap} denotes the collector aperture area, A_r is the receiver area, and F_R represent sthe heat removal factor. In addition, U_L expresses the overall heat loss coefficient of the collector, and S denotes the absorbed solar radiation. The collector aperture area is defined as follows:

$$A_{\mathrm{ap}} = (w - D)L\,, \tag{10}$$

in which, w is the width of the collector, D is the outer diameter of the glass cover and L is the length of the collector. The radiation absorbed by the receiver is equal to:

$$S = G_b \eta_r\,. \tag{11}$$

G_b is the solar radiation and η_r is the efficiency. The heat removal factor is obtained from:

$$F_R = \frac{\dot{m} C_{p,c}}{A_r U_L}\left[1 - \exp\left(-\frac{A_r U_L F_l}{\dot{m} C_{p,c}}\right)\right]. \tag{12}$$

$C_{p,c}$ is the specific heat of the oil in the receiver, and F_l is the collector efficiency factor, which is defined as

$$F_l = \frac{\dfrac{1}{U_L}}{\dfrac{1}{U_L} + \dfrac{D_{r,0}}{h_{fi}} + \dfrac{D_{r,0}}{2k}\ln\dfrac{D_{r,0}}{D_{r,i}}}\,. \tag{13}$$

The expression for the input heat in the linear parabolic solar collector is presented as follows:

$$Q_s = A_{\mathrm{ap}} G_b\,. \tag{14}$$

The efficiency of solar collectors' energy can be calculated using the equations presented by Duffy and Beckman [15] in the following manner:

$$\eta_{\mathrm{th,PTC}} = \frac{Q_u}{Q_s}\,. \tag{15}$$

The exergy of the solar collector is calculated using the equation provided below.

$$\dot{\mathrm{E}}\mathrm{x}_s = A_{\mathrm{ap}} G_b\left[1 + \frac{1}{3}\left(\frac{T_0}{T_s}\right)^4 - \frac{4}{3}\left(\frac{T_0}{T_s}\right)\right]. \tag{16}$$

The energy and exergy balance equations detailed in Table 2 can be used to determine the heat and power transferred, as well as the exergy destruction rate of each component in the proposed multigeneration system.

Table 2. Equations of energy balance and exergy destruction rate for each component of the proposed system.

Component	Energy balance equations	Exergy destruction rate equations
Solar collector	$\dot{m}_1 h_1 + \dot{Q}_u = \dot{m}_2 h_2$	$\dot{\mathrm{E}}\mathrm{x}_{D,\mathrm{col}} = \dot{\mathrm{E}}\mathrm{x}_{\mathrm{sun}} + \dot{\mathrm{E}}\mathrm{x}_1 - \dot{\mathrm{E}}\mathrm{x}_2$
ORC evaporator	$\dot{Q}_{\mathrm{eva,ORC}} = \dot{m}_2(h_2 - h_3) = \dot{m}_6(h_6 - h_9)$	$\dot{\mathrm{E}}\mathrm{x}_{D,\mathrm{eva,ORC}} = \dot{\mathrm{E}}\mathrm{x}_2 + \dot{\mathrm{E}}\mathrm{x}_9 - \dot{\mathrm{E}}\mathrm{x}_3 - \dot{\mathrm{E}}\mathrm{x}_6$
ORC turbine	$\dot{W}_{t,\mathrm{ORC}} = \dot{m}_6(h_6 - h_7)$	$\dot{\mathrm{E}}\mathrm{x}_{D,t,\mathrm{ORC}} = \dot{\mathrm{E}}\mathrm{x}_6 - \dot{W}_{t,\mathrm{ORC}} - \dot{\mathrm{E}}\mathrm{x}_7$
ORC TEG	$\dot{Q}_{\mathrm{TEG,ORC}} = \dot{m}_7(h_7 - h_8) = \dot{m}_{10}(h_{11} - h_{10})$	$\dot{\mathrm{E}}\mathrm{x}_{D,\mathrm{TEG,ORC}} = \dot{\mathrm{E}}\mathrm{x}_7 + \dot{\mathrm{E}}\mathrm{x}_{10} - \dot{\mathrm{E}}\mathrm{x}_8 - \dot{\mathrm{E}}\mathrm{x}_{11}$
ORC pump	$\dot{W}_{p,\mathrm{ORC}} = \dot{m}_8(h_9 - h_8)$	$\dot{\mathrm{E}}\mathrm{x}_{D,p,\mathrm{ORC}} = \dot{W}_{p,\mathrm{ORC}} - \dot{\mathrm{E}}\mathrm{x}_8 + \dot{\mathrm{E}}\mathrm{x}_9$
DEARC-High desorber	$\dot{Q}_{\mathrm{Hdes,DEARC}} = \dot{m}_3(h_3 - h_4)$	$\dot{\mathrm{E}}\mathrm{x}_{d,\mathrm{DEARC,Hdes}} = \dot{\mathrm{E}}\mathrm{x}_3 + \dot{\mathrm{E}}\mathrm{x}_{24} - \dot{\mathrm{E}}\mathrm{x}_4 - \dot{\mathrm{E}}\mathrm{x}_{25} - \dot{\mathrm{E}}\mathrm{x}_{28}$
DEARC-High condenser	$\dot{Q}_{\mathrm{Hcond,DEARC}} = \dot{m}_{28}(h_{28} - h_{29})$	$\dot{\mathrm{E}}\mathrm{x}_{d,\mathrm{Hcond,DEARC}} = \dot{\mathrm{E}}\mathrm{x}_{28} - \dot{\mathrm{E}}\mathrm{x}_{29}$
DEARC-Solution heat exchanger 1	$\dot{Q}_{\mathrm{SHX1,DEARC}} = \dot{m}_{15}(h_{15} - h_{16}) = \dot{m}_{13}(h_{14} - h_{13})$	$\dot{\mathrm{E}}\mathrm{x}_{d,\mathrm{SHX1,DEARC}} = \dot{\mathrm{E}}\mathrm{x}_{13} + \dot{\mathrm{E}}\mathrm{x}_{15} - \dot{\mathrm{E}}\mathrm{x}_{14} - \dot{\mathrm{E}}\mathrm{x}_{16}$
DEARC-Solution heat exchanger 2	$\dot{Q}_{\mathrm{SHX2,DEARC}} = \dot{m}_{25}(h_{25} - h_{26}) = \dot{m}_{23}(h_{24} - h_{23})$	$\dot{\mathrm{E}}\mathrm{x}_{d,\mathrm{SHX2,DEARC}} = \dot{\mathrm{E}}\mathrm{x}_{23} + \dot{\mathrm{E}}\mathrm{x}_{25} - \dot{\mathrm{E}}\mathrm{x}_{24} - \dot{\mathrm{E}}\mathrm{x}_{26}$
DEARC-Low condenser	$\dot{Q}_{\mathrm{Lcond,DEARC}} = \dot{m}_{18}h_{18} + \dot{m}_{30}h_{30} - \dot{m}_{19}h_{19} = \dot{m}_{31}(h_{32} - h_{31})$	$\dot{\mathrm{E}}\mathrm{x}_{d,\mathrm{Lcond,DEARC}} = \dot{\mathrm{E}}\mathrm{x}_{18} + \dot{\mathrm{E}}\mathrm{x}_{30} + \dot{\mathrm{E}}\mathrm{x}_{31} - \dot{\mathrm{E}}\mathrm{x}_{19} - \dot{\mathrm{E}}\mathrm{x}_{32}$
DEARC-Evaporator	$\dot{Q}_{\mathrm{eva,DEARC}} = \dot{m}_{21}(h_{21} - h_{20}) = \dot{m}_{35}(h_{36} - h_{35})$	$\dot{\mathrm{E}}\mathrm{x}_{d,\mathrm{eva,DEARC}} = \dot{\mathrm{E}}\mathrm{x}_{20} + \dot{\mathrm{E}}\mathrm{x}_{35} - \dot{\mathrm{E}}\mathrm{x}_{21} - \dot{\mathrm{E}}\mathrm{x}_{36}$
DEARC-Absorber	$\dot{Q}_{\mathrm{abs,DEARC}} = \dot{m}_{21}h_{21} + \dot{m}_{17}h_{17} - \dot{m}_{12}h_{12} = \dot{m}_{33}(h_{34} - h_{33})$	$\dot{\mathrm{E}}\mathrm{x}_{d,\mathrm{abs,DEARC}} = \dot{\mathrm{E}}\mathrm{x}_{21} + \dot{\mathrm{E}}\mathrm{x}_{17} + \dot{\mathrm{E}}\mathrm{x}_{33} - \dot{\mathrm{E}}\mathrm{x}_{12} - \dot{\mathrm{E}}\mathrm{x}_{34}$
DEARC-Pump 1	$\dot{W}_{p1,\mathrm{DEARC}} = \dot{m}_{12}(h_{13} - h_{12})$	$\dot{\mathrm{E}}\mathrm{x}_{d,p1,\mathrm{DEARC}} = \dot{W}_{p1,\mathrm{DEARC}} + \dot{\mathrm{E}}\mathrm{x}_{12} - \dot{\mathrm{E}}\mathrm{x}_{13}$
DEARC-Pump 2	$\dot{W}_{p2,\mathrm{DEARC}} = \dot{m}_{22}(h_{23} - h_{22})$	$\dot{\mathrm{E}}\mathrm{x}_{d,p2,\mathrm{DEARC}} = \dot{W}_{p2,\mathrm{DEARC}} + \dot{\mathrm{E}}\mathrm{x}_{22} - \dot{\mathrm{E}}\mathrm{x}_{23}$
PEM	$\dot{W}_{\mathrm{PEM}} = (\dot{m}_{42}h_{42} - \dot{m}_{43}h_{43} - \dot{m}_{44}h_{44})$	$\dot{\mathrm{E}}\mathrm{x}_{D,\mathrm{PEM}} = \dot{\mathrm{E}}\mathrm{x}_{42} + \dot{W}_{\mathrm{PEM}} - \dot{\mathrm{E}}\mathrm{x}_{43} - \dot{\mathrm{E}}\mathrm{x}_{44}$
DWH	$\dot{Q}_{\mathrm{DWH}} = \dot{m}_4(h_4 - h_5) = \dot{m}_{40}(h_{41} - h_{40})$	$\dot{\mathrm{E}}\mathrm{x}_{\mathrm{DWH}} = \dot{\mathrm{E}}\mathrm{x}_4 + \dot{\mathrm{E}}\mathrm{x}_{40} - \dot{\mathrm{E}}\mathrm{x}_5 - \dot{\mathrm{E}}\mathrm{x}_{41}$
RO	$\dot{W}_{\mathrm{RO}} = (\dot{m}_{37}h_{37} - \dot{m}_{38}h_{38} - \dot{m}_{39}h_{39})$	$\dot{\mathrm{E}}\mathrm{x}_{D,\mathrm{RO}} = \dot{\mathrm{E}}\mathrm{x}_{37} - \dot{\mathrm{E}}\mathrm{x}_{38} - \dot{\mathrm{E}}\mathrm{x}_{39}$
COP	$\mathrm{COP} = \dfrac{\dot{Q}_{\mathrm{eva,DEARC}}}{\dot{Q}_{\mathrm{Hdes,DEARC}} + \dot{W}_{\mathrm{net,DEARC}}}$	
Thermal efficiency	$\eta_{\mathrm{th,tot}} = \dfrac{\dot{W}_{\mathrm{ORC}} + \dot{W}_{\mathrm{TEG}} + \dot{Q}_{\mathrm{cooling}} + \dot{Q}_{\mathrm{DWH}} + \dot{m}_{43}\mathrm{HHV}_{\mathrm{H_2}} - \dot{W}_{\mathrm{PEM}} + \dot{m}_{38}h_{38} - \dot{W}_{\mathrm{RO}}}{\dot{Q}_u + \dot{m}_1 h_1}$	
Exergy efficiency	$\eta_{\mathrm{ex,tot}} = \dfrac{\dot{W}_{\mathrm{ORC}} + \dot{W}_{\mathrm{TEG}} + \dot{\mathrm{E}}\mathrm{x}_{\mathrm{cooling}} + \dot{\mathrm{E}}\mathrm{x}_{43} + \dot{\mathrm{E}}\mathrm{x}_{44} + \dot{\mathrm{E}}\mathrm{x}_{41} - \dot{\mathrm{E}}\mathrm{x}_{40} + \dot{\mathrm{E}}\mathrm{x}_{38}}{\dot{\mathrm{E}}\mathrm{x}_{\mathrm{in,sun}} + \dot{\mathrm{E}}\mathrm{x}_1}$	

3 Results and discussions

The analysis of thermodynamics relies on specific assumptions and input information. The system being discussed is based on the following assumptions:

- The system is in a state of steady operation.
- Heat loss from system boundaries is negligible.
- Potential and kinetic energy changes, as well as pressure loss in pipes and heat exchangers, are neglected.
- All turbines, pumps, condensers, and valves are assumed to operate as adiabatic systems.
- The condenser output streams are considered saturated liquid, while the evaporator output streams are assumed to be saturated vapor. Isentropic efficiency is evaluated for pumps and turbines.
- The absorber outlet and both desorber outlets are assumed to be in equilibrium.

- The assumption is that solar radiation is consistent and evenly distributed.
- It is assumed that geothermal hot water is uncontaminated and of high purity.

Table 3 shows the input parameters for system modeling. These parameters must be set initially before conducting any further calculations.

Table 3. Parameters for the current study's modeling need to be input.

Parameters	Unit	Value
Geothermal		
The temperature of the production well, T_1	°C	90
Solar [17]		
The collector width, w	m	5.76
The collector length, L	m	12.27
The outside diameter of receiver, $D_{o,r}$	m	0.07
The inlet temperature of receiver, T_{ri}	°C	90
Solar radiation intensity, G_b	W/m^2	850
RO [18]		
Recovery ratio, RR	-	0.3
Elements numbers, n_e	-	7
Pressure vessels numbers, n_v	-	42
Seawater salinity, X_f	g/kg	43
ORC [19, 20]		
Inlet pressure of turbine, P_6	kPa	3000
Outlet pressure of turbine, P_7	kPa	300
Turbine isentropic efficiency, $\eta_{t,\mathrm{ORC}}$	%	85
Pump isentropic efficiency, $\eta_{p,\mathrm{ORC}}$	%	80
PEM [21]		
$P_{\mathrm{H_2}}$, $P_{\mathrm{O_2}}$	atm	1
T_{PEM}	°C	80
$E_{\mathrm{act},a}$	kJ/mol	76
$E_{\mathrm{act},c}$	kJ/mol	18
λ_a	-	14
λ_c	-	10
D	mm	50
J_a^{ref}	A/m^2	1.7×10^5
J_c^{ref}	A/m^2	4.6×10^3
DEARC [22]		
Evaporative temperature, T_{eva}	°C	5
Condenser temperature, T_{con}	°C	35
Absorber temperature, T_{abs}	°C	35
Desorber temperature, T_{des}	°C	80
SHX	%	80

The absence of a specific arrangement documented in the literature prevents complete validation of the proposed system, necessitating validation on a subsystem basis. The validation of the double-effect absorption chiller introduced in this research has been conducted using the data presented by Herold et al [23].

Table 4. Validation of the double-effect absorption chiller with ref [23].

	This research	Ref [23]
COP	1.325	1.359
$Q_{\mathrm{evaporator}}$	354.2	360.6
Q_{desorber}	267.4	265.4

Upon examining the validation results, it is evident that the simulation results closely align with the references, indicating successful validation of the code. In the main sub cycles of the system under study, Figure 2 illustrates the exergy destruction rate. The solar collector clearly shows the highest rate of exergy destruction in both systems. After the solar collector, the ORC cycle has the second-highest exergy destruction rate in both systems. In the solar system, a significant portion of the solar radiation's exergy is dissipated into the environment as thermal waste from the solar collectors. One contributing factor to the elevated destruction rate in solar systems is the substantial temperature differential between the fluid entering the panel and its surface temperatures.

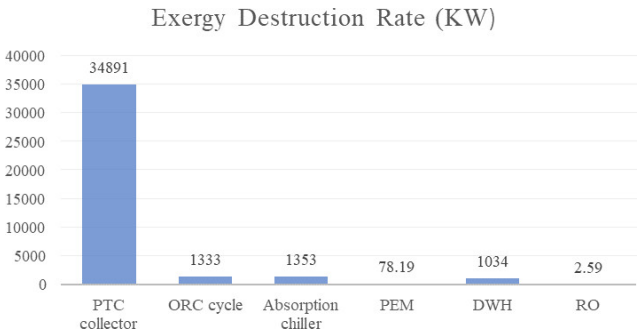

Fig. 2. Exergy destruction rate in the main sub cycles of the PTC-based system.

Figure 3 illustrates how the power output of the ORC turbine and the TEG unit is affected by the percentage of Al_2O_3 nanoparticles. The graph specifically presents the power generated by the TEG unit on the left and the power produced by the turbine. An analysis of the impact of the nanoparticle percentage in the nanofluid revealed that the power output of the ORC turbine increased, while the power generated by the TEG unit decreased. The temperature exiting the turbine decreases as the percentage of nanoparticles in the nanofluid increases, leading to a reduction in TEG power production. Inlet temperature greatly affects the performance of the TEG unit. For example, when the nanoparticle concentration is increased from 0 to 0.1, the power production rate of the ORC turbine increases from 67.93 kW to 68.21 kW, while the production rate of the TEG unit decreases from 66.03 kW to 63.53 kW.

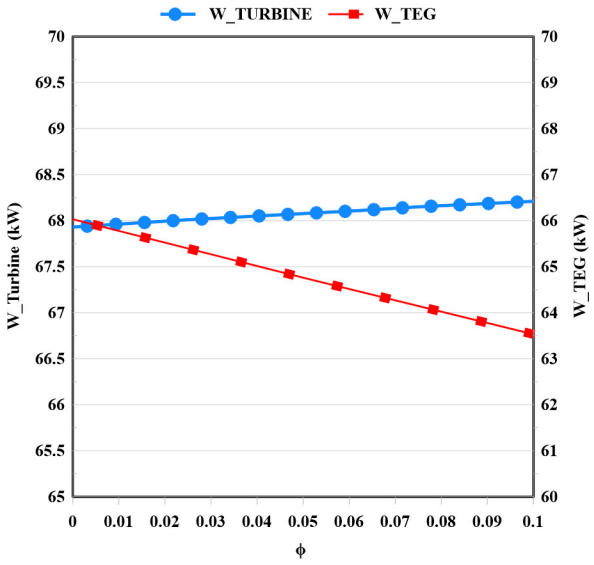

Fig. 3. The impact of nanoparticle volume concentration on the amount of power production rates in the turbine and TEG unit.

In Figure 4, we can see how changing the quantities of nanoparticles (ranging from 0% to 0.1%) affects the amount of useful energy gained from the PTC. When the nanoparticle percentage decreases, there is a corresponding decrease in the useful energy gain from the PTC. Specifically, utilizing Al_2O_3 nanoparticles resulted in a reduction in useful energy gain from 2761 kW to 2603 kW, which was linked to a decrease in the hydrogen production rate. This reduction in energy transferred to the ORC cycle suggests that in the absence of nanoparticles in the base fluid, the useful energy gain from the PTC was 2761 kW.

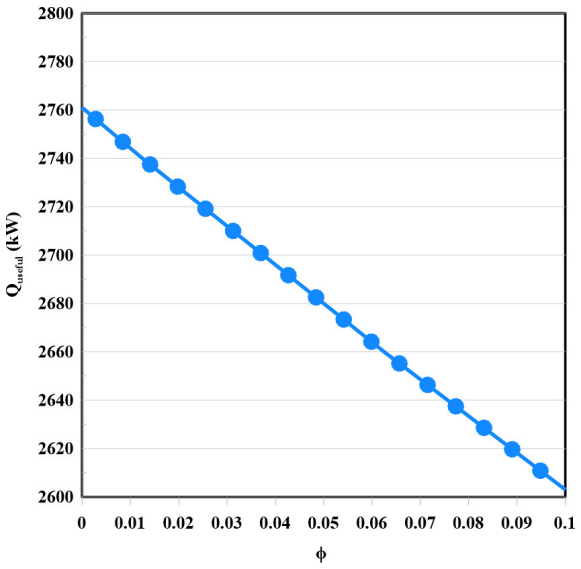

Fig. 4. The impact of nanoparticle volume concentration on the amount of useful energy gains from the PTC.

The PTC's effective energy gain is influenced by the solar irradiation it receives. Figure 5 demonstrates the correlation between solar irradiation and the PTC's useful energy gain, indicating a substantial increase in energy gain with higher solar irradiation levels. The utilization of Al2O3-based nanofluid led to an elevation in energy gain from 12591 KW to 14681 KW. This pattern of escalating energy gain is linked to the higher solar irradiation energy, resulting in a greater useful energy gain from the PTC.

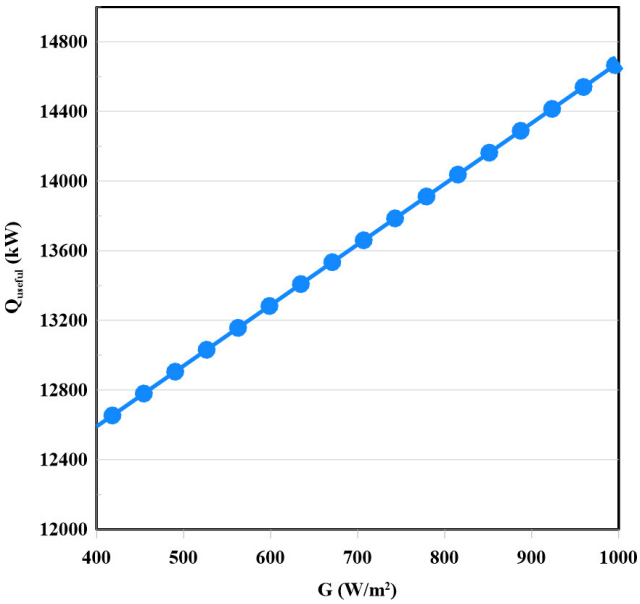

Fig. 5. The impact of solar radiation on the amount of useful energy gains from the PTC.

Figure 6 illustrates the correlation between solar irradiance and the rates of hydrogen and freshwater production, demonstrating an increase in production rates as solar irradiance levels rise. The increased production rates stem directly from the intensified solar irradiation, which enhances the solar energy's impact on the receiver, thereby raising the temperature of the working fluid exiting the PTC. This elevated exit temperature of the working fluid from the receiver tube enhances PTC efficiency and increases the heat output of the ORC cycle. As a result, this leads to higher output of power and increased rates of hydrogen and freshwater production. This enables more power to be supplied to the PEM electrolyzer and the RO unit. The rate of hydrogen production showed a significant increase with changes in solar irradiance, rising by 56.1%. Concurrently, freshwater production increased by 25%. Specifically, hydrogen production rose from 37.2 kg/day to 57.8 kg/day, and freshwater production went up from 1.188 kg/s to 1.485 kg/s.

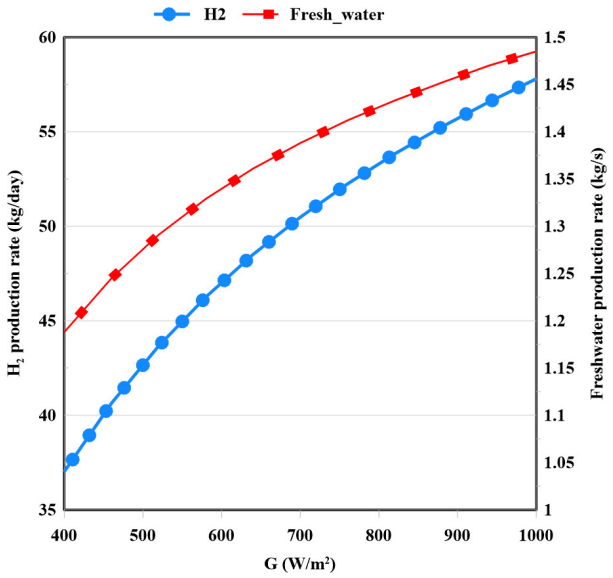

Fig. 6. The impact of solar irradiation on the amount of hydrogen and freshwater production rate.

Figure 7 illustrates the correlation between solar irradiance and power generation by the ORC turbine and TEG unit. As the solar radiation escalates from 400 W/m^2 to 1000 W/m^2, there is a noticeable escalation in power output from both the TEG unit and the ORC turbine, rising from 15.88 kW to 85.73 kW for TEG and from 53.41 kW to 85.73 kW for the ORC turbine. Increasing the solar radiation results in more energy being transferred to the ORC cycle, consequently leading to an overall augmentation in the power produced by the entire system.

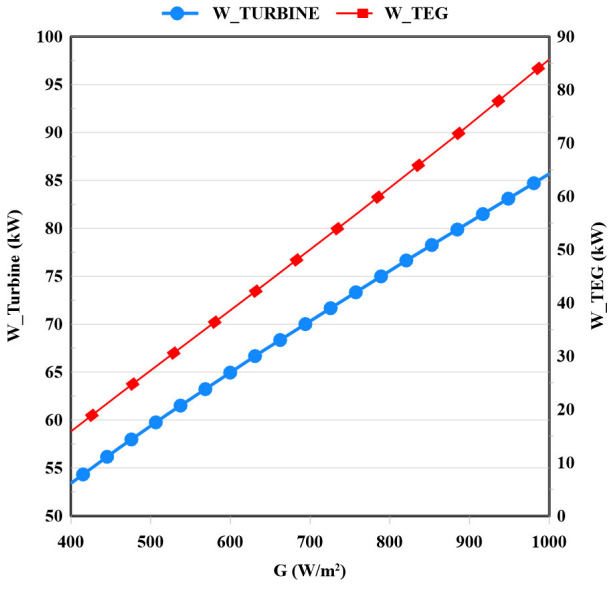

Fig. 7. The impact of solar irradiation on the amount of power produced by the system.

Figure 8 illustrates the impact of the collector inlet temperature on the system's hydrogen and freshwater production. An increase in the turbine inlet temperature leads to a higher production of hydrogen and freshwater by both the PEM electrolyzer and the RO unit. This is due to the fact that the rise in turbine inlet temperature causes an increase in the collector's outlet temperature, allowing for a greater transfer of energy to the sub cycles.

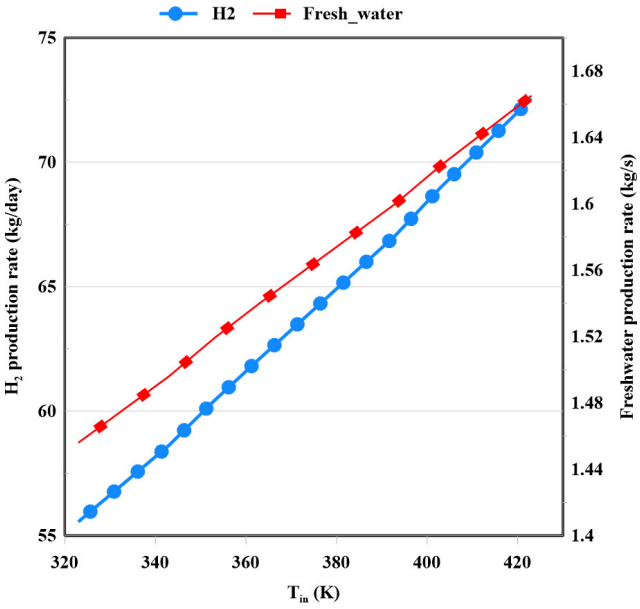

Fig. 8. The impact of the collector inlet temperature on the amount of hydrogen and freshwater production rate.

4 Conclusion

The research presents a multi-generational setup that can generate power, heat, cooling, hydrogen, and desalinated water concurrently. The following are the main results from the assessments of energy and exergy for this combined system. This groundbreaking setup is created to meet the energy, hydrogen, and clean water requirements of a zero-energy building. The condensed results of the thermodynamic examination, in line with the primary objectives of the system, are detailed below.

- The solar collector has the highest amount based on the exergy destruction analysis.
- Boosting the nanoparticle concentration leads to increased power output from the turbine and decreased electricity generation from the TEG.
- The collector's useful energy increases with higher solar irradiation but decreases with increasing nanoparticle percentage.

- As solar radiation intensity increases, both the turbine and TEG unit generate more power, resulting in higher rates of freshwater and hydrogen production.

References

[1] Xu C, Behrens P, Gasper P, Smith K, Hu M, Tukker A, et al. Electric vehicle batteries alone could satisfy short-term grid storage demand by as early as 2030. Nature Communications. 2023;14(1):119. 180

[2] Alrikabi N. Renewable energy types. Journal of Clean Energy Technologies. 2014;2(1):61–64. 180

[3] Nelson VC. Introduction to renewable energy. CRC press; 2011. 180

[4] Behzadi A, Habibollahzade A, Ahmadi P, Gholamian E, Houshfar E. Multi-objective design optimization of a solar based system for electricity, cooling, and hydrogen production. Energy. 2019;169:696–709. 180

[5] Verma SK, Tiwari AK, Chauhan DS. Experimental evaluation of flat plate solar collector using nanofluids. Energy conversion and Management. 2017;134:103–115. 180

[6] Dey S, Sreenivasulu A, Veerendra G, Rao KV, Babu PA. Renewable energy present status and future potentials in India: An overview. Innovation and Green Development. 2022;1(1):100006. 180

[7] Sezer N, Koç M. Development and performance assessment of a new integrated solar, wind, and osmotic power system for multigeneration, based on thermodynamic principles. Energy Conversion and Management. 2019;188:94–111. 180

[8] Bicer Y, Dincer I. Development of a new solar and geothermal based combined system for hydrogen production. Solar Energy. 2016;127:269–284. 180

[9] Alirahmi SM, Rostami M, Farajollahi AH. Multi-criteria design optimization and thermodynamic analysis of a novel multi-generation energy system for hydrogen, cooling, heating, power, and freshwater. International journal of hydrogen energy. 2020;45(30):15047–15062. 180

[10] Yuksel YE, Ozturk M. Thermodynamic and thermoeconomic analyses of a geothermal energy based integrated system for hydrogen production. International Journal of Hydrogen Energy. 2017;42(4):2530–2546. 180

[11] Wan P, Gong L, Bai Z. Thermodynamic analysis of a geothermal-solar flash-binary hybrid power generation system. Energy Procedia. 2019;158:3–8. 180

[12] Ayub M, Mitsos A, Ghasemi H. Thermo-economic analysis of a hybrid solar-binary geothermal power plant. Energy. 2015;87:326–335. 181

[13] Assareh E, Delpisheh M, Farhadi E, Peng W, Moghadasi H. Optimization of geothermal-and solar-driven clean electricity and hydrogen production multi-generation systems to address the energy nexus. Energy Nexus. 2022;5:100043. 181

[14] Duangthongsuk W, Wongwises S. An experimental study on the heat transfer performance and pressure drop of TiO2-water nanofluids flowing under a turbulent flow regime. International journal of heat and mass transfer. 2010;53(1-3):334–344. 181

[15] Ghasemi SE, Ranjbar AA. Thermal performance analysis of solar parabolic trough collector using nanofluid as working fluid: A CFD modelling study. Journal of Molecular Liquids. 2016;222:159–166. 181, 182

[16] Dudley V, Kolb G, Sloan M, Kearney D. SEGS LS2 solar collector test results, Report of Sandia National Laboratories. SANDIA94-1884, USA. 1994;. 181

[17] Al-Sulaiman FA. Exergy analysis of parabolic trough solar collectors integrated with combined steam and organic Rankine cycles. Energy Conversion and Management. 2014;77:441–449. 184

[18] Nafey A, Sharaf M. Combined solar organic Rankine cycle with reverse osmosis desalination process: energy, exergy, and cost evaluations. Renewable Energy. 2010;35(11):2571–2580. 184

[19] Khakrah H, Shamloo A, Kazemzadeh Hannani S. Determination of parabolic trough solar collector efficiency using nanofluid: a comprehensive numerical study. Journal of Solar Energy Engineering. 2017;139(5):051006. 184

[20] Tekkanat B, Yuksel YE, Ozturk M. The evaluation of hydrogen production via a geothermal-based multigeneration system with 3E analysis and multi-objective optimization. International Journal of Hydrogen Energy. 2023;48(22):8002–8021. 184

[21] Sabbaghi MA, Soltani M, Rosen MA. A comprehensive 6E analysis of a novel multigeneration system powered by solar-biomass energies. Energy. 2024;297:131209. 184

[22] Kaynakli O, Saka K, Kaynakli F. Energy and exergy analysis of a double effect absorption refrigeration system based on different heat sources. Energy Conversion and Management. 2015;106:21–30. 184

[23] Herold KE, Radermacher R, Klein SA. Absorption chillers and heat pumps. CRC press; 2016. 184